Mechanical efficiency of hydraulic air compressors

V. Pavese[a], D. Millar[b], and V. Verda[c]

[a] Department of Energy (DENERG), Politecnico di Torino, Torino, Italy,
valeria.pavese@studenti.polito.it
[b] Mining Innovation, Rehabilitation & Applied Research Corporation (MIRARCO), Sudbury (ON), Canada, dmillar@mirarco.org
[c] Department of Energy (DENERG), Politecnico di Torino, Torino, Italy, vittorio.verda@polito.it

Abstract:

The process of gas compression in the downcomer shaft or pipe of a hydraulic air compressor is nearly isothermal due to: i) the mass flow rate of water being typically of three orders higher than that of the gas it compresses, ii) water having a heat capacity approximately four times that of air, and iii) the intimate contact and large heat transfer area between the gas phase and the liquid phase of the bubbly flow. A formulation for estimation of the efficiency of a closed or open loop hydraulic air compressor, expressed in terms of the principal hydraulic air compressor design variables, is presented. The influence of a hitherto underappreciated factor affecting the performance of these installations, such as the solubility of the gas being compressed in the water, is explored. A procedure for estimating the yield of compressed gas, accounting for these solubility losses, is explained and used to determine the mechanical efficiency of historical hydraulic air compressor installations from reported performance data. The result is a significant downward revision of hydraulic air compressor efficiency by approximately 20 percentage points in comparison to most reported efficiencies. However, through manipulation of co-solute concentrations in the water, and the temperature of the water (through regulation of the ejection of compression heat), the mechanical efficiency can be increased to the formerly reported levels. The thermo-economic implication of these efficiency determinations is that in a modern context, hydraulic air compressors may be able to outperform conventional mechanical gas compression equipment.

Keywords:

Energy Efficiency, Compressed Air, Hydraulic Air Compressor, Isothermal Compression.

1. Introduction

In the late 19th and early 20th centuries Hydraulic Air Compressors were large scale installation typically formed in rock tunnels, that constituted a method of harnessing hydropower towards the production of compressed air firstly for cotton fabric production but then principally for mining industry applications [1]. A hydraulic air compressor is a device that is said to provide a practical isothermal compression process to the air that passes through it [2-4]. This paper aims to establish an expression for the mechanical efficiency of a HAC defined as:

$$\eta_{mech} = \frac{W_{ind}}{W_{input}} = \frac{\dot{W}_{ind}}{\dot{W}_{input}}, \qquad (1)$$

where W_{ind} is the indicated work, usefully delivered to the air when in its compressed state and W_{input} is the work supplied to the HAC system. W_{input} can be provided to the system in the form of hydropower in a natural watercourse, as illustrated in Fig. 1. Alternatively work may be provided to the system by a pump for the cases of an open or closed loop HAC [1]. In either cases, it is important to establish the mechanical efficiency of the system, especially in economic assessment studies involving comparisons with conventional air compression equipment, such as centrifugal compressors.

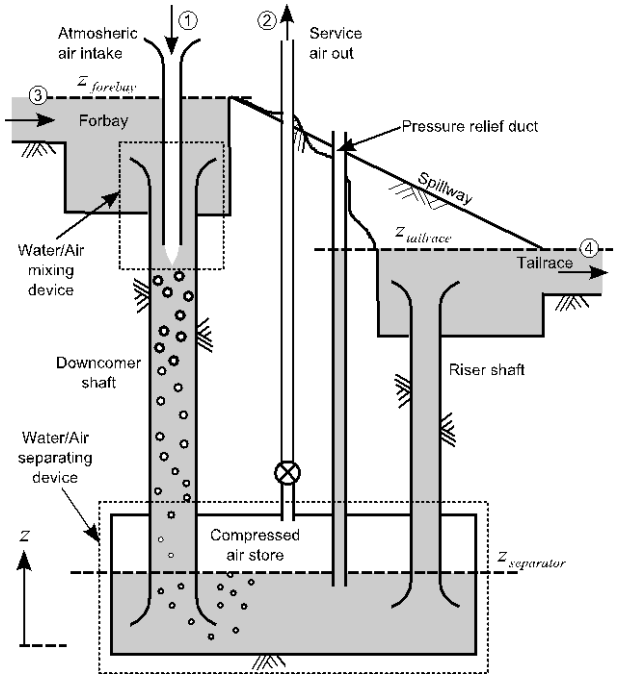

Fig. 1. Schematic of a hydraulic air compressor – station 1: air inlet; station 2: compressed air outlet; station 3: water inlet; station 4: water outlet.

2. Control volume formulation

Figure 2 shows a schematic of a HAC system that is considerably simplified in comparison to an actual HAC layout (Fig. 1). Air enters the control volume with mass flow rate $\dot{m}_{G,i}$ in 1 at $P_1 = P_{atm}$, $T_1 = T_{atm}$. Water enters the control volume with mass flow rate $\dot{m}_{W,i}$ in 3, with elevation $z_3 = z_{forebay}$ and $P_3 = P_{atm} = P_1$, $T_3 = T_{river}$. Air and water mass flows mix in a mixing device and as the water descends in the downcomer shaft, there is an interchange of work and heat between the two phases before the pressurized two-phase flow is separated into individual air and water phases in a water/air separation device. Water ascends the riser shaft and leaves the control volume at the tailrace elevation, $z_4 = z_{tailrace}$, facing atmospheric pressure $P_4 = P_{atm} = P_1 = P_3$ and at temperature T_4. Service air leaving the HAC exits from section 2 at a pressure determined by the difference in water level elevation at the tailrace of the HAC and the water level elevation at the water-air separator system at depth, $P_2 = \rho_W g\left(z_{tailrace} - z_{separator}\right) + P_{atm}$. The temperature of the service air is the same as the temperature of the water in the tailrace, $T_2 = T_4$.

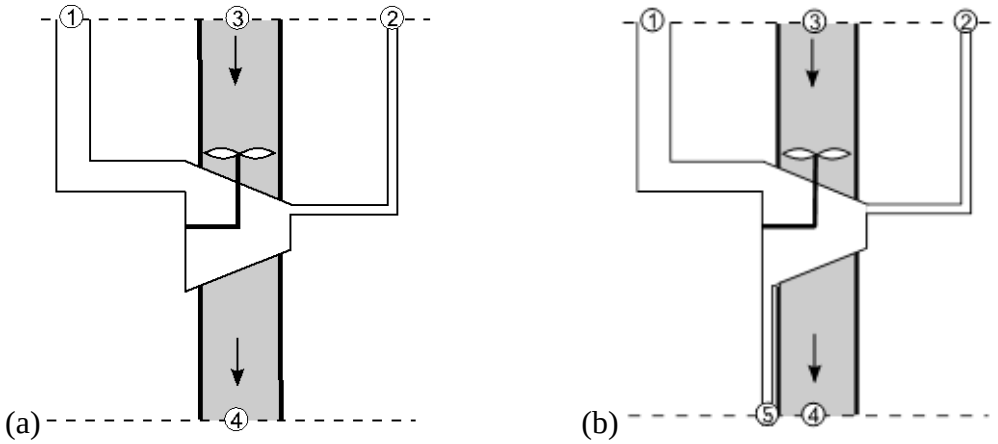

Fig. 2. Control volume schematic of a HAC (a) for 1st law analysis (b) for analysis where gases dissolve in the water, by-pass the gas-liquid separator and return to atmosphere via the riser.

Note that Fig. 2 is a highly stylized representation of the HAC system that ignores the vertical extent of the processes ongoing within the HAC at depth that is more apparent in Fig. 1. Figure 2 could be taken to apply to a rather more conventional air compressor that possesses a water jacket transferring heat away from the air as it is compressed, with a water mass flow rate sufficient to remove heat from the air, so that the air always attains the temperature of the water. Fig. 2 also attempts to illustrate that the compression work done on the air arises from 'harnessing' the potential energy loss of the water, as it flows through the 'water jacket', by means of the stylization of the mechanical element connected to the compressor .

To determine the mechanical work added to the air (supplied by the water) per kg of air, w_{12}, the input work to the air is recognized as arising from the change in potential energy, as the water falls from station 3 to 4:

$$\dot{m}_G w_{12} = \dot{m}_W g(z_3 - z_4), \qquad (2)$$

so that, the work added to the air is

$$w_{12} = \frac{\dot{m}_W g(z_3 - z_4)}{\dot{m}_G}, \qquad (3)$$

This is not the same as the indicated work per kg of the service air delivered, which will be discussed subsequently. Adopting a convention of heat and work being added to a flow as positive, the steady flow energy equation (SFEE) is considered between the respective input and output locations for the air and the water phases separately. For the air:

$$\frac{v_{1G}^2 - v_{2G}^2}{2} + g(z_1 - z_2) + w_{12} + q_{12} = h_{2G} - h_{1G}, \qquad (4)$$

and the control volume is drawn such that the locations of input and output states of air have the same elevation (for the air), and the diameters of the ducts containing the air at these locations are assumed engineered so that velocity $v_{1G} = v_{2G}$. Note that these conditions are not quite the same as assuming the difference between the velocities and the difference between elevations are negligible, but have a similar effect, so that:

$$w_{12} + q_{12} = h_{2G} - h_{1G}, \qquad (5)$$

Solving (5) for q_{12} and substituting (3) yields:

$$q_{12} = (h_{2G} - h_{1G}) - \frac{\dot{m}_W}{\dot{m}_G} g(z_3 - z_4), \qquad (6)$$

The SFEE can be applied to the water flow assuming the forbay and tailrace geometries carefully engineered so that $v_{3W} = v_{4W}$, and:

$$w_{34} + q_{34} = h_{4W} - h_{3W} - g(z_3 - z_4), \qquad (8)$$

where w_{34} denotes the mechanical work supplied by the water to the air (i.e. leaving the water), one obtains another perfect statement of the first law and q_{34} the heat added to the water during the compression, per unit mass of water, therefore:

$$q_{34} = (h_{4W} - h_{3W}) - g(z_3 - z_4) - w_{34}, \qquad (9)$$

The thermal interaction between the two phases can be represented as:

$$\dot{m}_W q_{34} + \dot{m}_G q_{12} = 0, \qquad (10)$$

Solving (10) for q_{34} and substituting (6) yields:

$$q_{34} = -\frac{\dot{m}_G}{\dot{m}_W} q_{12} = -\frac{\dot{m}_G}{\dot{m}_W}\left(h_{2G} - h_{1G}\right) + g\left(z_3 - z_4\right), \qquad (11)$$

and from (9) and (11) the mechanical work w_{34} results:

$$w_{34} = h_{4W} - h_{3W} + \frac{\dot{m}_G}{\dot{m}_W}\left(h_{2G} - h_{1G}\right) - 2g\left(z_3 - z_4\right), \qquad (12)$$

For a perfectly isothermal process for the water $h_{4W} = h_{3W}$ since $P_4 = P_3$ and $T_4 = T_3$. Practically, in a HAC although T_4 may be close to T_3 they cannot be identical because heat is added to the water in the process, which must increase its temperature. Consequently, in the foregoing, the enthalpy terms in (11) and (12) must be retained in considering this a *nearly isothermal process* for the water, rather than a *perfectly isothermal process*.

With the exception of specific times when the river and atmospheric air temperatures are the same, air temperature will vary from atmospheric temperature at inlet, to the temperature of the river water at exit. After the mixing process at the HAC inlet, temperatures of air and water can be taken to be the same, and thereafter, as the two-phase flow descends, work and heat transfers will occur *nearly isothermally*. For air, generally rather than specifically, the sequential processes of mixing and nearly isothermal compression will lead to an overall process best described as polytropic. The mechanical efficiency of the compression of air by a HAC can be expressed, e.g. [5,6] as:

$$\eta_{mech} = \frac{W_{ind}}{W_{input}} = \frac{\int_1^2 V dP}{w_{12}}, \qquad (18)$$

where the useful pneumatic work yielded up by the compressed air as it is consumed, is:

$$\int_1^2 V dP = R\left(T_2 - T_1\right)\frac{\ln\left(P_2/P_1\right)}{\ln\left(T_2/T_1\right)}, \qquad (19)$$

so that by substituting (19) and (3) into (18) one obtains:

$$\eta_{mech} = \frac{R\left(T_2 - T_1\right)\dfrac{\ln\left(P_2/P_1\right)}{\ln\left(T_2/T_1\right)}}{\dfrac{\dot{m}_W}{\dot{m}_G} g\left(z_3 - z_4\right)}, \qquad (20)$$

Recalling that $P_1 = P_{atm}$, $P_2 = \rho_W g\left(z_{tailrace} - z_{separator}\right) + P_{atm}$, $T_1 = T_{atm}$, $T_3 = T_{river}$, $T_2 = T_4$ and defining $T_4 - T_3 = \delta T$ as a small temperature change of the water through a HAC with operating head $H = \left(z_3 - z_4\right)$, efficiency can be written in terms of the on-site observables:

$$\eta_{mech} = \frac{R\left(T_{river} + \delta T - T_{atm}\right)\dfrac{\ln\left[\left(\rho_W g\left(z_{tailrace} - z_{separator}\right) + P_{atm}\right)/P_{atm}\right]}{\ln\left(\left(T_{river} + \delta T\right)/T_{atm}\right)}}{\dfrac{\dot{m}_W}{\dot{m}_G} gH}, \qquad (21)$$

To determine δT the work interaction between the two phases can be represented as:

$$\dot{m}_W w_{34} + \dot{m}_G w_{12} = 0, \qquad (22)$$

and by substituting (12) and (3) into (22), making substitutions of the form $h = C_p T$ and solving for δT, one obtains:

$$\delta T = \frac{\frac{\dot{m}_W}{\dot{m}_G} gH - C_{pG}\left(T_{river} - T_{atm}\right)}{C_{pG} + \frac{\dot{m}_W}{\dot{m}_G} C_w}, \qquad (23)$$

which can be used to establish the HAC efficiency (21). For a HAC with given available head and a fixed depth to the separator water level from the tailrace level, δT depends upon environmental temperatures at input with just the input mass flow rates as control variables. Practically, the historic HACs were regulated by adjusting the mass flow of the water entering the system, leaving the mass flow of air as a free variable that adjusted itself to the physics.

3. The effect of solubility on HAC mechanical efficiency

Effectiveness of the system is affected by the solubility of gas species in water [1]. Historical HAC installations reported a reduced oxygen concentration in the compressed air being observed during their use in mines [7]. This occurred because gaseous air species dissolved in the water passing through HACs and thus by-passed the air-water separation systems. In formulations of efficiency that relied on mass continuity of the air between the (low pressure) inlet and (high pressure) outlet (sections 1 and 2 in Fig. 1), the useful pneumatic power delivered by the compressor,

$$\dot{W}_{ind} = \dot{m}_G \int_1^2 V dP, \qquad (24)$$

was overestimated because the value of $\dot{m}_G$ used in the calculation did not account for the gas solubility losses. In re-analysis of the published information on HAC efficiency, the mass flow at inlet, $\dot{m}_{G,in}$, must be distinguished from that at outlet, $\dot{m}_{G,out}$. A compressed air yield parameter, y, then arises from the HAC efficiency equation:

$$\eta_{mech} = \frac{\dot{W}_{ind}}{\dot{W}_{input}} = \frac{\dot{m}_{G,out} \int V dp}{\dot{m}_{G,in} w_{12}} = \frac{\dot{m}_{G,out}}{\dot{m}_{G,in}} \cdot \frac{\int V dp}{w_{12}} = y \cdot \frac{\int V dp}{w_{12}}, \qquad (25)$$

To properly establish the mechanical efficiency of a HAC, the mass flow of the gas dissolved in the water must be determined, ideally using the same set of on-site observables, as used previously. The problem of its determination is complicated by three factors:

1) The solubility of a gas in a liquid is directly proportional to the partial pressure of the gas above the liquid (Henry's law) and reduces with increasing temperature.
2) When an air bubble is entrained within the water of the HAC, it becomes isolated from the atmosphere. During compression of an air bubble, the equilibrium that the solubility parameter characterizes is established between the finite mass of gas within the closed boundary of the air bubble, and the water phase around it and the partial pressure of the gas varies as the mass of gas in the bubble depletes.
3) The process of solution of a gas in a liquid is known to be affected by the kinetics of the process. Rate equations are needed to establish how close the concentrations of the gas dissolved within the water actually are to a new, higher pressure, equilibrium state.

The required calculations can be simplified by assuming that the residence time of a bubble in the separation chamber is sufficiently long that the composition of the bubble gas chemistry has come to equilibrium with the dissolved gas species, which makes factor 3 as negligible. Gas species solubility at atmospheric pressure is required to determine the mass of dissolved gas species at the water inlet to the HAC given the partial pressures of those species in the atmosphere. It is also

required for the HAC delivery pressure, which is determined exactly from the head between the HAC tailrace elevation and the elevation of the gas-water interface in the HAC separation device. An iterative procedure is used to establish the gas species solubility at depth, due to the constraint that gas dissolving in the water when pressure rises, must be drawn from the finite mass of gas drawn into the water at inlet. This alters the partial pressures of the gas species in the bubbles in a non-trivial manner such that, ultimately, a new dynamic equilibrium is established with the concentrations of the dissolved gas species, dictated by the solubility of these gases at the new temperature and pressure. The net effect is a mass transfer of the gas species from the bubbles to the water, which accounts for the 'by-pass loss' of the HAC and permits direct estimation of *y*. The interested reader is referred to [8] for details of the iterative procedure, flow charts, and code listings of the algorithm.

4 Efficiency determination of precedent HAC installations

Considering all available data identified in the literature regarding precedent HAC systems [1,11,12], their mechanical efficiency can be estimated using (21), (23) and (25).

The results are shown in Table 1 and for more detailed performance testing reported [1,11,15] in Appendix B. Table 1 constitutes a revision of HAC efficiency values reported by Langborne [12].

The input data for calculations are temperature and pressure of the fluids at the compressor intake, the depth of the riser shaft, the mass flow rate of water and air, and the yield parameter, that is, the on-site observables. Where possible, a detailed examination of the historical weather records was undertaken to establish reasonable values for the input temperatures and pressures.

The maximum theoretical efficiency is obtained with yield equal to 100%. By comparing these with values of HAC efficiency presented in the literature, it is possible to deduce whether or not the corresponding performance tests metered the air mass flow rate at the HAC inlet or at the point of air delivery (as summarized in the last column of Table 1). In some cases, the disparities between the literature values and those computed (accounting for yield) are striking. In the case of the Victoria Mine HAC, the efficiencies are 20% less, whereas the values of the maximum, theoretical efficiency computed for this work are consistent with the literature values.

The mass flow rate ratio, $\dot{m}_W / \dot{m}_G$, is a parameter that could be controlled by the operator by means of control valves for both fluid streams, and the magnitude of the delivery pressure of a HAC is a design parameter that reflects the air-water separator depth. The product of these two parameters was chosen for the abscissa of the plot showing the variation of efficiency for the various historical HACs, firstly without the yield and secondly with the yield (Fig. 3). With this choice of abscissa, the optimum efficiency HAC design appears to be embodied by the Cascade, Dillingen, and Glanzenberg HAC installations, with $\left(\dot{m}_W / \dot{m}_G\right) \cdot \left(\rho_W g\left(z_{tailrace} - z_{separator}\right) + P_{atm}\right)$ = 900,000 kPa and maximum theoretical efficiencies of 95.67%, 94.08% and 91.43%, respectively.

Introducing the yield parameter estimated from the on-site observables, the overall efficiencies are reduced from 50 - 95% to 35 - 82%. In particular for the three installations with highest mechanical efficiency, the overall mechanical efficiency drops to 82.41% 78.09%, and 72.98% for Dillingen, Cascade and Glanzenberg respectively.

Table 1. Comparison between the calculated value of mechanical efficiencies and values presented in literature. Underlined figures in the tables are efficiencies lower than those previously reported.

No.	Year	Location	Design Parameters		Temperatures		Pressure		Mass flow rate			Yield	Efficiency			Intake / Delivery
			Available head (m)	Riser depth (m)	Water (°C)	Air (°C)	Atm (kPa)	Delivery (kPa)	Water inlet (kg/s)	Air inlet (kg/s)	Air outlet (kg/s)	(%)	Mechanical (%)	Overall (%)	Literature value (%)	
1	1896	Dominion Cotton Mills, Magog, Quebec, Canada [13]	6.58	36.55	25	26.67	101.3	458.5	2907.9	0.793	0.577	72.77	54.71	39.82	55	I
2	1898	Ainsworth, British Columbia, Canada [13,11]	32.77	61.11	15	15	101.3	700.1	1980.2	2.949	2.643	89.64	74.10	66.42	53	I
3	1898	Dillingen Ironworks, Dillingen, Sear, Germany [11]	1.80	12.39	15	15	101.3	222.8	867.2	0.203	0.176	86.87	86.51	75.15	79	D
4	1901	Cascade Range, Washington State, USA [11]	13.72	60.05	15	15	101.3	689.6	1414.4	1.147	0.937	81.62	95.67	78.09		D
5	1902	Norwich, Conn., USA [13]		57.00	15	15	101.3	659.8								
6	?	Peru [14]														
7	1903	Glanzenberg Mine, Nr Siegen, Germany I [15,11]	40	82.58	15	15	101.3	910.4	14.2	0.026	0.023	88.79	86.01	76.37	74	D
8	1903	Glanzenberg Mine, Nr Siegen, Germany II [15,11]	50	72.30	15	15	101.3	809.7	14.7	0.033	0.030	91.80	78.07	71.67	70	D
9	1903	Glanzenberg Mine, Nr Siegen, Germany III [15,11]	17	72.30	15	15	101.3	809.7	14.2	0.013	0.010	79.81	91.43	72.98	70.2	D
10	1904	Trent Canal Lift Lock, Peterborough, Ontario, Canada [11]	2.74	19.67	15	15	101.3	294.1								D
11	1905	Holzappel, Germany [11]	117.04	64.04	15	15	101.3	728.8	17.9	0.091	0.088	96.78	72.12	69.80	66	D
12	1906	Victoria Mine, Ontonagon County, Michigan, USA [12,16]	21.34	79.55	10.94	12	96.5	876.3	20964.9	20.00	15.68	78.36	82.20	64.41	82	I
13	1907	Royal Mine Inspection Plant, Clausthal, Germany [15,11]	99.30	50	15	15	101.3	591.2	53.3	0.210	0.203	96.73	59.18	57.24	77	D
14	1908?	Zeche Victor Rauxel Mine, Dortmund, Germany [15,11]	82	61.57	15	15	101.3	704.6	66.6	0.213	0.202	95.05	63.82	60.66	73	D
15	1909	Royal Mine Inspection Plant, Grund, Germany [11]	36	61.85	15	15	101.3	707.3	157.0	0.261	0.236	90.59	75.66	68.54	88	D
16	1909	Ragged Chutes, Nr Cobalt, Ontario, Canada [19, 17]	16.92	83.97	21	21	101.3	923.2	29690.4	22.65	17.09	75.42	85.81	64.71	83	I
17	1915	Persberg, Sweden [11]	29.57					790.3	2.4						45-57	
18	1924?	Cumberland, England [11]														
19	1925	Falun, Sweden [18]	47.85	79.55	15	15	101.3	880.8	179.8	0.343	0.307	89.46	72.72	65.06	46-52	I
20	1929	Saragossa, Spain [11]	1.83		25	25	101.3	204.3	2831.4							
21	1929	Nigeria, Tin mine [11]														

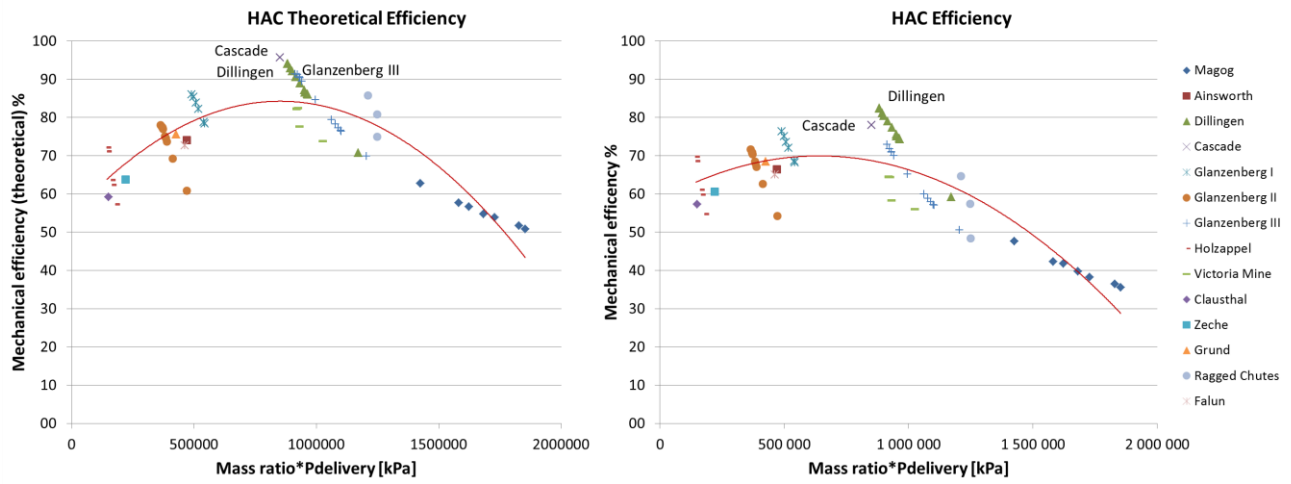

Fig. 3. Theoretical and overall mechanical efficiency of 14 hydraulic air compressor installations, plotted against the product of the mass ratio of the two phase (water, air) bubbly flow and delivery pressure.

It is of historical interest that Charles Taylor, the HAC patent's owner, had a wager with the owners of Victoria Mine (Michigan, USA) that was based on the as-built performance of the HAC he supplied to them. For every 3% efficiency points lower than 70%, Taylor agreed to accept $1,000 less of his fee. Because of Taylor's efficiency guarantee, the compressor was tested on May 28 and 29, 1906 and on the basis of these tests (reproduced in [11]), he won the bet. The measured efficiency reported [11] varies between 73.50 and 82.27% and agrees well with the theoretical efficiency computed herein (Table 1), that is, the efficiency that does not account for gas yield. With the yield estimated and the overall mechanical efficiency of the installation recomputed, the actual efficiency of the Victoria Mine compressor is estimated as ranging from 56.01 to 64.50%. These results suggest that during tests at Victoria Mine the mass flow rate was metered at the inlet of the compressor instead of at the outlet, so the air mass lost during the process was neglected. They also suggest that Taylor should have lost his bet!

5. Approach from an exergetic point of view

A correct description of the process that takes place in a HAC must consider a small increase in gas temperature to drive the exchange of heat between air and water. As energy is converted from potential energy to heat and work exchanged between the two fluids, further analysis of the process is required, namely one that considers not only the amount of energy involved but also the quality of energy exchanged. A description of the system that includes the First and the Second Law of Thermodynamics together leads to a more complete interpretation of HAC system behaviour. In particular, exergy analysis is a well-established method for the design, optimization, and performance evaluation of energy systems [20,21].

Exergy analysis is adopted to take into account the different thermodynamic values of different energy forms and quantities, that is, the work and heat transferred, and to determine the lost work or irreversibility of the process. The thermodynamic imperfections can be quantified as exergy destructions, which represent losses in energy quality or usefulness. The destruction of exergy is proportional to the rate of entropy generation, $\dot{S}_{gen}$, where the coefficient of proportionality is the reference temperature, T_0. This quantity can be evaluated by means of the exergy balance applied to a defined control volume. For an open system, adopting again the convention of heat and work being added to a flow as positive, the exergy balance in steady state can be written as:

$$\sum_{i=1}^{N} \dot{Q}_i \left(1 - \frac{T_0}{T_i}\right) + \dot{W} = \sum_{k=1}^{NC} \pm \dot{m}_k b + T_0 \dot{S}_{gen}, \qquad (26)$$

where the two terms on the right hand side express the exergy related to the thermal flow, exchanged with a heat source at temperature T_i, and the mechanical-electric power, while on the left hand side, the first term is referred to mass flows entering or leaving the system and the last term is the flux of destroyed exergy. *N* is the total number of heat flows and *NC* is the number of streams crossing the system.

Excluding nuclear, magnetic, electrical and interfacial effects, the exergy of a stream of substance crossing the system boundary is given by the sum of the kinetic, potential, physical and chemical exergy [21]. Thus, according to [22], the specific exergy of a mass flow is:

$$b = \frac{v^2}{2} + gz + b_{ph} + b_{ch}, \qquad (27)$$

The physical exergy is calculated from the reference state at temperature T_0 and pressure p_0 without any change of the chemical composition of the considered substance:

$$b_{ph} = h - h_0 - T_0(s - s_0), \qquad (28)$$

The chemical exergy [22] expresses the exergy content of the substance at environmental temperature and pressure and its value results from the difference of composition of this substance in relation to the commonly appearing components of the environment. The chemical part of exergy can be expressed by means of chemical potential μ_i and molar mass M_i of species *i*

$$b_{ch} = \sum_i \frac{1}{M_i}(\mu_{i,0} - \mu_{i,00}), \qquad (29)$$

The quantity $\mu_{i,0}$ denotes the value of μ at the restricted dead state (i.e., when the system is in thermal and mechanical, but not chemical, equilibrium with the environment), with intensive properties T_0, p_0 and mole fraction x_i for each species *i*. The intensive properties $\mu_{i,00}$, T_0, p_0 and $x_{i,0}$ characterize the conceptual reference environment, denoted as dead state, within which the system is in complete equilibrium.

For gaseous substances containing only the gaseous species present in the reference environment, the calculation of chemical exergy takes into account only the change of the concentration of the components of the considered substance [22]:

$$b_{ch} = h_{i,0} - h_{i,00} - T_0(s_{i,0} - s_{i,00}) = T_0 \sum_i f_i R_i \ln \frac{x_i}{x_{i,0}}, \qquad (30)$$

where f_i and x_i denote the mass and mole fraction of species *i*, respectively.

Applying the exergy balance (26) to the control volume in Fig. 2a, it is possible to determine the rate of irreversibility produced in the HAC when no losses of compressed air are present and the yield parameter assumes value equal to 100%:

$$T_0 \dot{S}_{gen} = \dot{m}_G(b_{1G} - b_{2G}) + \dot{m}_W(b_{3W} - b_{4W}) + \dot{Q}_d\left(1 - \frac{T_0}{T}\right), \qquad (31)$$

The last term in (31) disappears if the temperature of the external environment is equal to that of the reference state. Assuming again proper engineered ducts for air and water flows, so that $v_{1G} = v_{2G}$ and $v_{3W} = v_{4W}$, the variation in specific exergy for air and water results in:

$$b_{1G} - b_{2G} = h_{1G} - h_{2G} - T_0(s_{1G} - s_{2G}), \qquad (32)$$

$$b_{3W} - b_{4W} = g(z_3 - z_4) + h_{3W} - h_{4W} - T_0(s_{3W} - s_{4W}), \qquad (33)$$

It can be noted that the specific chemical exergy is characterised by the same value at inlet and outlet locations since, if the chemical concentrations of substances present remain unchanged.

However to take into account the effect of the solubility previously explained, the portion of air that comes out of solution in the riser shaft can be represented as an additional flow of air leaving the control volume at the tailrace elevation and at the same temperature and pressure of the water at section 4. Hence, the control volume that must be considered for the application of the exergy balance is the one shown in Fig. 2b. The schematic in Fig. 2b does not represent the process of dissolution in water and separation to which the flow of air leaving the system is subjected at section 5 with elevation $z_3 = z_4 = z_{tailrace}$ and state $P_5 = P_4 = P_{atm}$, $T_5 = T_4$.

Introducing the yield parameter, the exergy destroyed can be evaluated as:

$$T_0 \dot{S}_{gen} = \dot{m}_G b_{1G} - y \cdot \dot{m}_G b_{2G} - (1-y) \cdot \dot{m}_G b_{5G} + \dot{m}_W (b_{4W} - b_{3W}) + \dot{Q}_d \left(1 - \frac{T_0}{T}\right). \qquad (34)$$

It is important to highlight that the variation of the solubility, as previously described, affects the partial pressures of gases that constitute the compressed air mixture. Gaseous species that form the air mixture leaving the system at station 2 and 5 have different mass and mole fractions than at section 1. This phenomenon leads to a variation of the chemical potential, and thus of the chemical exergy, of the air flow from the inlet to the outlet locations. Whereas (33) is still valid for the variation of specific exergy of the water flow, the specific exergy of air mixture at sections 1, 2 and 5 can be assessed with respect to the reference state conditions as follows:

$$b = \frac{v^2}{2} + gz + \sum_i f_i \left(h_i - h_{i,0} - T_0 \left(s_i - s_{i,0}\right)\right) + T_0 \sum_i f_i R_i \ln \frac{x_i}{x_{i,0}}, \qquad (35)$$

As stated in [20] and [22], the physical exergy can be decomposed in two contributions in order to separate the role of pressure and temperature. The third term on the right hand side of (35) can be divided into thermal exergy, b_{phT}, and mechanical exergy, b_{php}:

$$b_{phT} = \sum_i f_i \left[h_i(T, p_i) - h_i(T_0, p_i) - T_0 \left(s_i(T, p_i) - s_i(T_0, p_i)\right)\right], \qquad (36)$$

$$b_{php} = \sum_i f_i \left[h_i(T_0, p_i) - h_i(T_0, p_{i,0}) - T_0 \left(s_i(T_0, p_i) - s_i(T_0, p_{i,0})\right)\right], \qquad (37)$$

These two quantities are determined by the change in enthalpy and entropy of the mixture from operational states, with T, p, x_i for each species i to the restricted dead state at T_0, P_0, x_i for each species i, so that the reference partial pressure, $p_{i,0}$, is given by the product of the pressure P_0 and the mole fraction x_i. The variation on the gases' mole fractions, passing from the restricted dead state to the dead state at T_0, P_0, $x_{i,0}$ for each species i, is included in the last term of (35).

Expressing (36) and (37) for an ideal gas mixture and substituting the third term of the right hand side in (35), the specific exergy of air flows can be evaluated as:

$$b = \frac{v^2}{2} + gz + \sum_i f_i C_{p,i} \left(T - T_0 - T_0 \ln \frac{T}{T_0}\right) + T_0 \sum_i f_i R_i \ln \frac{p_i}{p_{i,0}} + T_0 \sum_i f_i R_i \ln \frac{x_i}{x_{i,0}} \qquad (38)$$

Considering that the partial pressure p_i is given by the product of the pressure P and the mole fraction x_i of species i, the last two terms in (38) can be rearranged as in equation (39) and (40):

$$b = \frac{v^2}{2} + gz + \sum_i f_i C_{p,i} \left(T - T_0 - T_0 \ln \frac{T}{T_0}\right) + T_0 \sum_i f_i R_i \ln \frac{x_i P}{x_i P_0} \cdot \frac{x_i}{x_{i,0}}, \qquad (39)$$

$$b = \frac{v^2}{2} + gz + \sum_i f_i C_{p,i} \left(T - T_0 - T_0 \ln \frac{T}{T_0} \right) + T_0 \sum_i f_i R_i \ln \frac{x_i P}{x_{i,0} P_0}, \quad (40)$$

In addition to the rate of irreversibility produced in the system, the exergetic efficiency or rational efficiency [21] of the system can be established, that is, the ratio of the useful exergetic effect to the consumption of the driving exergy (used exergy).

For a HAC system, the used exergy is given by the change in exergy content of the water flow. This quantity is mainly determined by the change in potential energy undergone by the water flowing from section 3 to section 4, that is, the first term on the right hand side in (33). Whereas, in HACs the useful exergy effect is given by the change in exergy content of the air flow compressed. The exergy efficiency for a HAC undergoing a theoretical process, that is, with yield of 100%, can be obtained by:

$$\eta_{ex} = \frac{\dot{m}_G \left(b_{2G} - b_{1G} \right)}{\dot{m}_W \left(b_{3W} - b_{4W} \right)}, \quad (41)$$

In real processes taking place in HACs, the solubility effect must be taken into account and the exergetic efficiency assumes the following expression:

$$\eta_{ex} = \frac{y \cdot \dot{m}_G \left(b_{2G} - b_{1G} \right)}{\dot{m}_W \left(b_{3W} - b_{4W} \right)}. \quad (42)$$

Equation (42) implies that the exergy of the air flow leaving the system at station 5 is considered as an exergy waste emission.

Data available regarding historical HAC installations (summarized in Table 1) are used to establish the irreversibility production and the exergetic efficiency of the system. Dead state conditions, chosen for the analysis, are reported in Table 2. The temperature *T* of the heat source, toward which the dissipated heat is released in the present case of imperfect insulation of the system, is assumed to be equal to the temperature of the reference environment T_0. This approximation does not strongly affect the result since the value of $\dot{Q}_d$, evaluated by applying the First Law of Thermodynamics to the overall system, was negligible with respect to the calculated flux of destroyed exergy. Mass and mole fractions of gas species at sections 2 and 5, needed for the determination of exergy content of air flow, are obtained by means of the iterative procedure [8] used to establish the yield parameter.

Exergetic efficiencies that include the effect of solubility are shown in graphical form in Fig. 4. The highest values of exergy efficiency are 81.81% and 78.47%, corresponding to Dillingen and Cascade installations respectively. Exergy efficiencies appear close to calculated energy efficiencies. Hence, installations with a higher energy performance are also characterized by higher performance from the point of view of the Second Law.

Table 2. Dead state conditions. Mass and mole fraction are obtained by normalization of typical values for standard dry atmosphere [9,10]

Temperature	$T_0 = 298.15\,\mathrm{K}$		
Pressure	$p_0 = 1\,\mathrm{atm}$		
Composition	Atmospheric dry air at T_0 and p_0 having the following composition:		
	Air constituents	Mole fraction	Mass fraction
	N_2	0.7808131	0.7551365
	O_2	0.2094528	0.2313835
	Ar	0.0093397	0.0128807
	CO_2	0.0003944	0.0005993

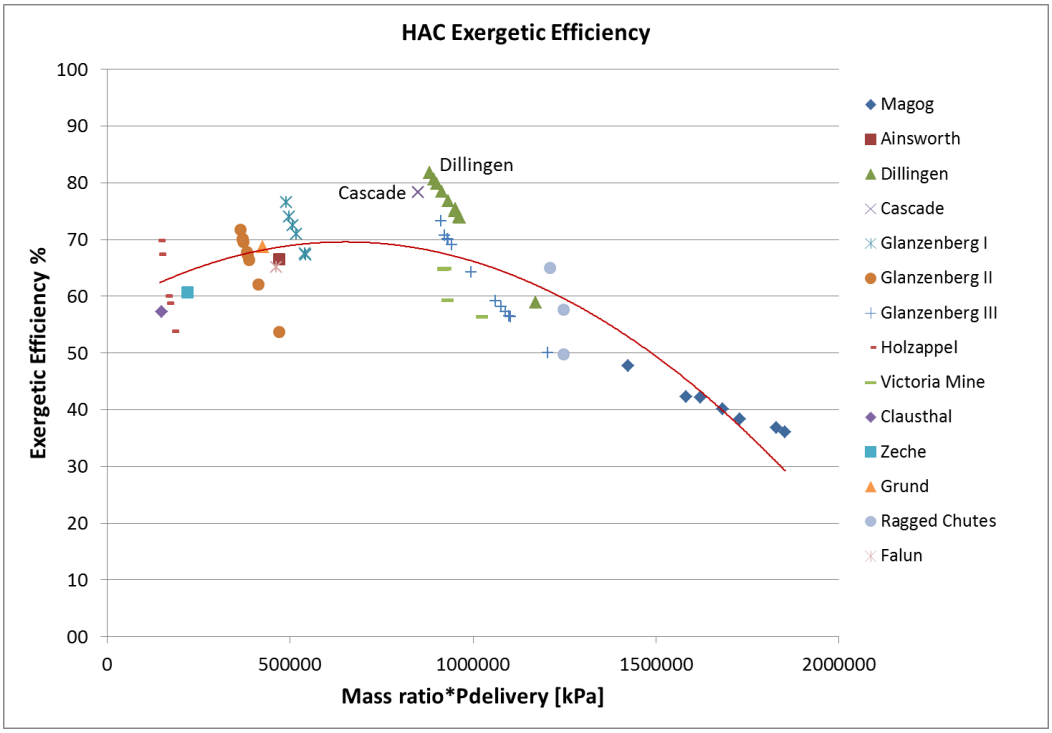

Fig. 4. HAC exergetic efficiency of 14 hydraulic air compressor installations plotted against the product of the mass ratio of the two phase (water, air) bubbly flow and delivery pressure.

The rate of irreversibility production presented in Fig. 5 is normalized to the value of water flow rate in order to give a better comparison between installations with different design parameters that result in strong differences of water mass flow rate. The highest absolute value of flux of exergy destruction came from the Ragged Chutes and Victoria Mine installations, while, by analysing the normalized value of exergy consumption, Holzappel and Clausthal were the cases where the highest irreversibility was produced (considering the amount of water mass flow involved in the system, that is, the scale of the compressor). Installations with the highest values of Second Law efficiency are found to be characterized by the lowest values of normalized exergy consumption, as evident in Fig. 5.

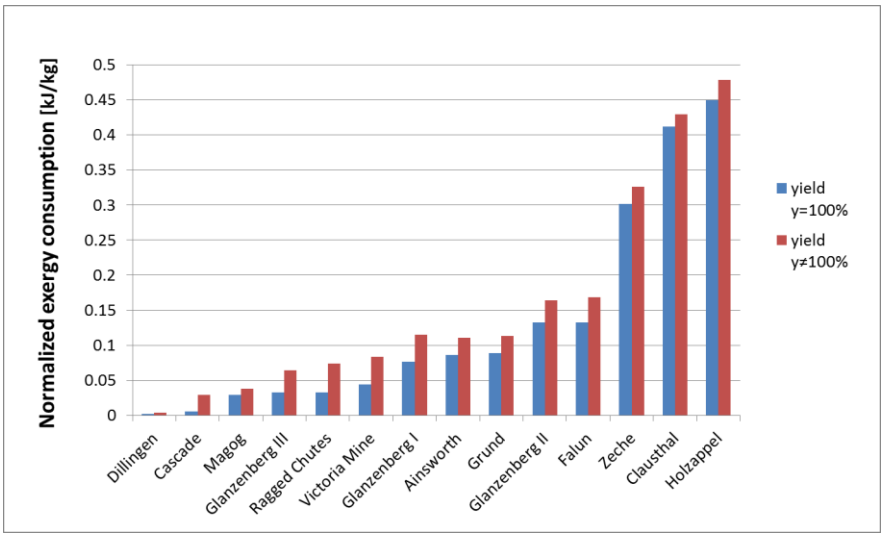

Fig. 5. Rate of irreversibility production of 14 hydraulic air compressor installations normalized to the water mass flow rate. Mean results are presented for installations with several test conditions available (see Table A, appended).

6. Conclusion

This paper proposes an energy and exergy based analysis of the processes taking place in a HAC. The expression of HAC energy efficiency derived by considering a so called *nearly isothermal* process gives a more precise description of the system, as compared with those proposed in previous analyses using an isothermal compression. The important role of air solubility during the compression process is presented and the methodology used to evaluate its effect is described in detail. The evaluation of theoretical and actual HAC efficiencies, which takes into account the effect of solubility, were computed and compared with data available in the literature for all installations of proven existence. The exergetic analysis permits the rate of irreversibility produced in the system and the Second Law efficiency to be evaluated, in order to give a comparison between different HAC installations.

Acknowledgments

This work was developed under the outgoing mobility program founded by Politecnico di Torino. Thanks are extended to the hosting organisations: Mining Innovation, Rehabilitation & Applied Research Corporation (MIRARCO) and Laurentian University in Sudbury, ON, Canada.

References

[1] Millar D., A review of the case for modern-day adoption of hydraulic air compressors. Applied Thermal Engineering 2014;69(1-2):55-77.

[2] Bidini G., Grimaldi C.N., and Postrioti L., Performance analysis of a hydraulic air compressor. Proceedings of the Institution of Mechanical Engineers Part A, Journal of Power and Energy, 1999;213(A3):191-203.

[3] Rice W., Performance of hydraulic gas compressor. Transactions of the ASME, Journal of Fluids Engineering 1976;96:645-653.

[4] Nishi A., Highly efficient gas turbine system using isothermal compression. JSME International Journal Series B, Fluids and Thermal Engineering 1996;39(3):615-620.

[5] McPherson M.J., Subsurface Ventilation and Environmental Engineering. London: Chapman & Hall; 1993

[6] Rogers G.F.C., Mayhew Y.R. Engineering thermodynamics: work and heat transfer. London: Longman; 1967

[7] E.B.W., Report on oxygen content of hydraulic air compressor at Ragged Chutes. Mines & Minerals 1910;31(3).

[8] Pavese V., Energy and Exergy analysis of a Hydraulic Air Compressor for application in the mining industry [dissertation]. Torino, Italy: Politecnico di Torino; 2015

[9] Glueckauf, E., The composition of atmospheric air. In: Malone, T.F. editor. Compendium of Meteorology. Boston, MA: American Meteorological Society. 1951. pp. 3–10.

[10] Tans P, Keeling R., Trends in carbon dioxide: Global CO_2 Data 2013 – Available at <http://www.esrl.noaa.gov/gmd/ccgg/trends/global.html#global_data> [accessed 21.10.2014].

[11] Schulze Leroy E., Hydraulic Air Compressors. Washington, DC: United States Department of Interior, Bureau of Mines, Information Circular 7683. 1954.

[12] Langborne P.L., Hydraulic air compression: old invention – new energy source. Chartered Mechanical Engineer 1979;26(10):76-81

[13] Peele P., Compressed Air Plant, fifth ed. New York: John Wiley & Sons; 1930.

[14] Anonymous, Charles Havelock Taylor (Obituary), Canadian Mining and Metallurgical Bulletin 1950;191-203.

[15] Bernstein P., Hydraulic compressors (In German), Z. Ver. Dtsch. Ing. 1910;54(45):1903-1908.

[16] Hartenberg R.S., Denavit J., The fabulous air compressor, Machine Design 1960;32(15):168-170.

[17] Auclair A., Ragged chutes, Canadian Mining Journal 1957;78(8):98-101.

[18] Markman B.G., The hydraulic compressor station at the Falue mine, Jernkontorets Annaler 1928;10:497-517.

[19] Taylor C.H., Cobalt hydraulic air compressor, Mines Minerals 1910;30(9):532-534

[20] Kotas T.J., The Exergy Method of Thermal Plant Analysis. London: Butterworths; 1985.

[21] Szargut J., Morris D.R., Steward F.R., Exergy analysis of thermal, chemical and metallurgical processes. New York: Hemisphere Publ. Corp; 1988.

[22] Szargut J., Exergy method: technical and ecological applications. Southampton, Boston: WIT Press; 2005.

Nomenclature

b specific exergy, J/kg
C specific heat capacity, J/(kg K)
f mass fraction
g acceleration of gravity, m/s^2
h specific enthalpy, J/kg
H hydraulic head, m
$\dot{m}$ mass flow rate, kg/s
M molar mass, g/mol
n polytropic exponent
p_i partial pressure of i, kPa
P pressure, kPa
q specific heat transfer, J/kg
$\dot{Q}$ heat transfer rate, kW
R gas constant, J/(kg K)
s specific entropy, J/kg
$\dot{S}$ rate of entropy generation, kW/K
T temperature, °C
v velocity, m/s
V specific volume, m^3/kg
w specific work, J/kg
W work, kJ
$\dot{W}$ rate of work, kW
x mole fraction
y yield
z elevations

Greek symbols

δT temperature difference, K
η energy efficiency
ρ density, kg/m^3
μ chemical potential, J/mol

Subscripts and superscripts

00 dead state
0 restricted dead state
atm atmospheric
ch chemical
d dissipated
ex exergetic
G gaseous phase
i gas species
in inlet
ind indicated
input input
mech mechanical
out outlet
ph physical
p constant pressure
T constant temperature
W liquid phase

Table A. Mechanical and overall efficiency calculated for HAC installations with test conditions available in literature [1,11,15].

Location	Design Parameters		Temperatures		Pressure		Mass flow rate			Yield	Efficiency	
	Available head (m)	Riser depth (m)	Water (°C)	Air (°C)	Atm (kPa)	Delivery (kPa)	Water inlet (kg/s)	Air inlet (kg/s)	Air outlet (kg/s)	(%)	Mechanical (%)	Overall (%)
Magog - Test 1	6.5	36.7	26.1	24	101.3	459.9	2881.5	0.767	0.544	70.94	53.85	38.2
Magog - Test 3	6.8	36.7	26.7	24.2	101.3	459.9	1885	0.608	0.462	75.94	62.79	47.68
Magog - Test 5	6.6	36.7	25	26.7	101.3	459.9	2968.8	0.842	0.62	73.67	56.73	41.8
Dillingen Ironworks - Test 1	1.8	12.4	20	14	101.3	222.9	415.7	0.079	0.066	83.7	70.81	59.26
Dillingen Ironworks - Test 3	1.8	12.4	20	14	101.3	222.9	521.6	0.127	0.111	87.15	90.65	79
Dillingen Ironworks - Test 5	1.8	12.4	20	14	101.3	222.9	656.5	0.164	0.143	87.44	92.85	81.19
Dillingen Ironworks - Test 7	1.8	12.4	20	14	101.3	222.9	767.4	0.19	0.166	87.34	92.09	80.43
Dillingen Ironworks - Test 9	1.8	12.4	20	14	101.3	222.9	847.4	0.199	0.172	86.66	87.23	75.59
Glanzenberg I - Test 1	40	82.7	21.8	12	101.3	911.9	9	0.015	0.013	87.07	78.39	68.26
Glanzenberg I - Test 3	40	82.7	21.8	12	101.3	911.9	14.2	0.026	0.023	88.04	85.33	75.13
Glanzenberg I - Test 5	40	82.7	21.8	12	101.3	911.9	16.7	0.028	0.025	87.06	78.74	68.56
Glanzenberg II - Test 1	50	72.4	20.5	13.5	101.3	810.6	8.7	0.015	0.013	89.21	60.82	54.26
Glanzenberg II - Test 3	50	72.4	20.5	13.5	101.3	810.6	11.4	0.024	0.022	91.05	73.71	67.11
Glanzenberg II - Test 5	50	72.4	20.5	13.5	101.3	810.6	13.8	0.03	0.028	91.46	77.45	70.84
Glanzenberg II - Test 7	50	72.4	20.5	13.5	101.3	810.6	15.1	0.033	0.03	91.41	76.99	70.37
Glanzenberg II - Test 9	50	72.4	20.5	13.5	101.3	810.6	18	0.038	0.035	91.15	75.11	68.46
Glanzenberg III - Test 1	17	72.4	22	12	101.3	810.6	7	0.005	0.004	74.93	77.31	57.93
Glanzenberg III - Test 3	17	72.4	22	12	101.3	810.6	9.3	0.007	0.005	75.21	78.24	58.84
Glanzenberg III - Test 5	17	72.4	22	12	101.3	810.6	11.8	0.01	0.008	78.46	90.55	71.04
Glanzenberg III - Test 7	17	72.4	22	12	101.3	810.6	14.2	0.012	0.01	78.62	91.25	71.74
Glanzenberg III - Test 9	17	72.4	22	12	101.3	810.6	17.6	0.013	0.01	75.58	79.38	59.99
Glanzenberg III - Test 11	17	72.4	22	12	101.3	810.6	19.6	0.013	0.01	72.41	69.91	50.62
Holzappel - Test 1	117	64.1	19.5	9.5	101.3	729.5	18	0.09	0.087	96.41	71.17	68.62
Holzappel - Test 3	117	64.1	19.5	9.5	101.3	729.5	32.2	0.141	0.136	95.9	62.43	59.87
Victoria Mine - Test 1	21.5	80.2	10.9	12	96.5	882.5	6159.2	5.912	4.63	78.31	82.36	64.5
Victoria Mine - Test 3	21.5	80.2	10.9	12	96.5	882.5	5996.3	5.163	3.92	75.92	73.77	56.01

Location	Mass fraction N2		Mass fraction O2		Mass fraction Ar		Mass fraction CO2		Useful Exergy	Used Exergy	Rate of Irreversibility	Theoretical Exergy Efficiency	Useful Exergy	Used Exergy	Rate of Irreversibility	Exergy Efficiency
	Stn 2 (%)	Stn 5 (%)	Stn 2 (%)	Stn 5 (%)	Stn 2 (%)	Stn 5 (%)	Stn 2 (%)	Stn 5 (%)	(kW)	(kW)	(kW)	(%)	(kW)	(kW)	(kW)	(%)
Magog - Test 1	79.48	65.83	19.46	32.12	1.06	1.85	0.00	0.20	99.20	184.94	85.73	53.64	70.88	184.94	113.55	38.33
Magog - Test 3	78.91	64.78	19.99	33.06	1.09	1.92	0.00	0.24	78.74	125.97	47.23	62.50	60.15	125.97	65.43	47.75
Magog - Test 5	79.15	65.33	19.77	32.55	1.07	1.89	0.00	0.22	108.91	191.50	82.59	56.87	80.75	191.50	110.20	42.17
Dillingen Ironworks - Test 1	77.76	63.97	21.05	33.88	1.17	1.91	0.02	0.25	5.35	7.64	2.29	70.07	4.50	7.64	3.10	58.90
Dillingen Ironworks - Test 3	77.37	62.90	21.42	34.81	1.19	1.97	0.02	0.33	8.60	9.59	0.99	89.65	7.52	9.59	2.01	78.41
Dillingen Ironworks - Test 5	77.34	62.79	21.45	34.88	1.19	1.97	0.02	0.36	11.08	12.07	0.99	91.82	9.73	12.07	2.27	80.57
Dillingen Ironworks - Test 7	77.36	62.81	21.44	34.85	1.19	1.97	0.01	0.38	12.85	14.11	1.26	91.07	11.26	14.11	2.76	79.82
Dillingen Ironworks - Test 9	77.44	63.02	21.37	34.66	1.18	1.96	0.01	0.36	13.44	15.58	2.14	86.28	11.69	15.58	3.79	75.05
Glanzenberg I - Test 1	77.64	61.30	21.19	36.21	1.18	2.04	0	0.46	2.85	3.70	0.85	77.00	2.48	3.70	1.20	67.23
Glanzenberg I - Test 3	77.48	61.03	21.33	36.42	1.18	2.05	0	0.50	4.89	5.83	0.94	83.81	4.31	5.83	1.50	73.97
Glanzenberg I - Test 5	77.63	61.28	21.20	36.22	1.18	2.04	0	0.46	5.30	6.86	1.55	77.34	4.63	6.86	2.21	67.53
Glanzenberg II - Test 1	77.30	60.85	21.50	36.53	1.19	2.07	0	0.55	2.67	4.44	1.77	60.07	2.38	4.44	2.05	53.71
Glanzenberg II - Test 3	77.02	60.34	21.77	36.91	1.21	2.09	0	0.66	4.23	5.82	1.58	72.78	3.86	5.82	1.94	66.39
Glanzenberg II - Test 5	76.90	60.61	21.82	37.23	1.21	2.11	0.06	0.05	5.38	7.04	1.66	76.47	4.93	7.04	2.10	70.04
Glanzenberg II - Test 7	76.92	60.60	21.82	37.21	1.21	2.11	0.06	0.09	5.86	7.70	1.85	76.01	5.36	7.70	2.33	69.58
Glanzenberg II - Test 9	76.99	60.29	21.80	36.94	1.21	2.09	0	0.68	6.81	9.18	2.37	74.16	6.22	9.18	2.94	67.73
Glanzenberg III - Test 1	79.33	64.12	19.59	33.75	1.09	1.89	0	0.24	0.93	1.22	0.29	75.92	0.70	1.22	0.52	57.21
Glanzenberg III - Test 3	79.30	64.04	19.62	33.82	1.09	1.90	0	0.24	1.25	1.62	0.38	76.83	0.94	1.62	0.67	58.11
Glanzenberg III - Test 5	78.85	63.36	20.04	34.43	1.11	1.93	0	0.28	1.83	2.06	0.23	88.89	1.44	2.06	0.61	70.09
Glanzenberg III - Test 7	78.83	63.33	20.06	34.45	1.11	1.93	0	0.28	2.22	2.48	0.26	89.58	1.75	2.48	0.71	70.77
Glanzenberg III - Test 9	79.21	64.09	19.66	33.89	1.09	1.90	0.04	0.12	2.39	3.07	0.68	77.95	1.82	3.07	1.24	59.22
Glanzenberg III - Test 11	79.61	64.75	19.29	33.25	1.07	1.86	0.03	0.14	2.35	3.42	1.07	68.67	1.71	3.42	1.70	50.02
Holzappel - Test 1	76.13	59.02	22.57	38.48	1.26	2.14	0.05	0.35	15.25	21.82	6.57	69.88	14.71	21.82	7.09	67.41
Holzappel - Test 3	76.23	58.87	22.49	38.18	1.25	2.13	0.03	0.83	23.92	39.02	15.10	61.31	22.96	39.02	16.02	58.84
Victoria Mine - Test 1	78.88	63.35	20.01	34.44	1.11	1.93	0.00	0.27	1118.90	1356.67	237.77	82.47	880.03	1356.67	471.47	64.87
Victoria Mine - Test 3	79.20	63.88	19.70	33.97	1.09	1.91	0.00	0.25	977.04	1322.69	345.65	73.87	745.32	1322.69	572.66	56.35